Integrated Ferroelectrics
An International Journal

ISSN: (Print) (Online) Journal homepage: https://www.tandfonline.com/loi/ginf20

The Mechanical, Electronic and Optical Properties of $Sn_2P_2S_6$ Compound in Different Phases

Husnu Koc, Selami Palaz, Sevket Simsek, Amirullah M. Mamedov & Ekmel Ozbay

To cite this article: Husnu Koc, Selami Palaz, Sevket Simsek, Amirullah M. Mamedov & Ekmel Ozbay (2021) The Mechanical, Electronic and Optical Properties of $Sn_2P_2S_6$ Compound in Different Phases, Integrated Ferroelectrics, 220:1, 56-70, DOI: 10.1080/10584587.2021.1921535

To link to this article: https://doi.org/10.1080/10584587.2021.1921535

Published online: 01 Dec 2021.

Submit your article to this journal

Article views: 43

View related articles

View Crossmark data

Full Terms & Conditions of access and use can be found at
https://www.tandfonline.com/action/journalInformation?journalCode=ginf20

INTEGRATED FERROELECTRICS
2021, VOL. 220, 56–70
https://doi.org/10.1080/10584587.2021.1921535

Taylor & Francis
Taylor & Francis Group

Check for updates

The Mechanical, Electronic and Optical Properties of $Sn_2P_2S_6$ Compound in Different Phases

Husnu Koc[a], Selami Palaz[b], Sevket Simsek[c], Amirullah M. Mamedov[d,e], and Ekmel Ozbay[d]

[a]Department of Physics, Faculty of Science and Letters, Siirt University, Siirt, Turkey; [b]Department of Physics, Faculty of Sciences, Harran University, Sanliurfa, Turkey; [c]Department of Material Science and Engineering, Faculty of Engineering, Hakkari University, Hakkari, Turkey; [d]Nanotechnology Research Center, Bilkent University, Ankara, Turkey; [e]International Scientific Center, Baku State University, Baku, Azerbaijan

ABSTRACT

In present paper, the structural, mechanical, and electronic properties of the Sn2P2S6 compound under different pressures by the density functional methods in the generalized gradient approximation have been examined in the ferroelectric (Pc) and paraelectric (P2_1/c) phases. The lattice parameters, mechanical properties, electronic bands structures and partial density of states for both phases are presented and analyzed. The nonlinear optical properties and electro-optic effects of Sn2P2S6-Pc have been studied by the density functional theory in the local density approximation. Our structural estimation and some other results are in agreement with the available experimental and theoretical data. We present calculations of the frequency-dependent complex dielectric function (ω) and the second harmonic generation response coefficient $\chi^{(2)}$ (-2ω, ω, ω) over a large frequency range. The electronic linear electro-optic susceptibility $\chi^{(2)}$ ($-\omega$, ω, 0) is also evaluated below the band gap. These results are based on a series of the LDA calculation. The results for $\chi^{(2)}$ ($-\omega$, ω, 0) are in agreement with the experiment below the band gap and those for $\chi^{(2)}$ ($-\omega$, ω, 0) are compared with the experimental data where available.

ARTICLE HISTORY
Received 23 November 2020
Accepted 25 March 2021

KEYWORDS
Ab initio calculation; electronic structure; mechanical properties; optical properties

1. Introduction

In 1965, $M_2P_2X_6$ transition metal hypodithiophosphates were first reported by Hahn and Klingen. Where M is a transition metal and X is a sulfur or selenium. The researchers reported that $Sn_2P_2S_6$ compound crystallize in orange and transparent polyhedra and have a Pc space group with $a = 5.63$ Å, $b = 7.47$ Å, $c = 11.03$ Å, and $\beta = 122.2°$ lattice parameters. In 1973, Klingen, Ott, and Hahn reported that the $Sn_2P_2S_6$ compound had three different phases: 1 rhombohedral and 2 monoclinic. They labeled the monocillic phase as monocillic (I) and monocillic (II). In 1974, Dittmar and Schaifer reported that $Sn_2P_2S_6$ was a monocillic (II) structure at room temperature, and had a Pn (equivalent to Pc) space group with $a = 9.378$ Å, $b = 7.488$ Å, $c = 6.513$ Å and

CONTACT Amirullah M. Mamedov mamedov@bilkent.edu.tr
© 2021 Taylor & Francis Group, LLC

$\beta = 91.15^{\circ}$ lattice parameters. In 1974, Carpentier and Nitsche concluded that the monocillic (II) $Sn_2P_2S_6$ crystals showed the ferrolectric behavior and that the polarization axis was in the [101] direction and the Curie temperature was 66 °C [1–6].

Recent research on ferroelectric crystal $Sn_2P_2S_6$ has been motivated by both basic and practical problems [7, 8]. The $Sn_2P_2S_6$ crystal passes a second order phase from the room temperature ferroelectric phase to the high temperature paraelectric Pn/21 phase having an inversion center at $T_c \approx 377$ K. The $Sn_2P_2S_6$ structure is characterized by PS_3–PS_3 distances (P–S and P–P are 2.2 Å and 2.0 Å, respectively) held together by S–Sn interactions. Sn–S distance at high temperatures varies between 2.91 and 2.93 Å. Therefore, inversion symmetry is maintained around the midpoint between two Sn atoms. In the room temperature phase (ferroelectric phase), this inversion symmetry is broken because the range of Sn–S distances is 2.78–3.46 Å around an Sn atom and 2.88–3.52 Å around the others [8, 9].

In the literature review, it is understood that experimental and theoretical studies [6–8, 10–16] on $Sn_2P_2S_6$ compounds have been done. As far as we know, it has not been determined that the theoretical studies on the mechanical, linear and nonlinear optical properties of $Sn_2P_2S_6$ compounds have been performed. In this study, structural, mechanical, electronic and optical (linear and nonlinear) properties of $Sn_2P_2S_6$ compounds have been investigated.

2. Method of Calculation

Simulations of $Sn_2P_2S_6$ compound were conducted, using two different quantum mechanical density functional theory (DFT) programs. The first quantum mechanical DFT package program [17] used in the calculations is VASP (Vienna ab-initio simulation program) [18–21]. The exchange-correlation energy function in this package program is treated within the GGA (generalized gradient approximation) by the density functional of Perdew et al. [22]. The potentials used for the GGA calculations take into account the $5s^2 5p^2$ [Kr] valence electrons of each Sn-, $3s^2 3p^3$ valence electrons of each P-, and $3s^2 3p^4$ [Ne] valence electrons of each S-atoms. When including a plane-wave basis up to a kinetic-energy cutoff equal to 15.8 Ha for $Sn_2P_2S_6$ compound, the properties investigated in this work are well converged. The Brillouin-zone integration was performed using special k points sampled within the Monkhorst–Pack scheme [23]. We found that a mesh of $6 \times 5 \times 4$ k points for this compound was required to describe the structural, mechanical and electronic properties. This k-point mesh guarantees a violation of charge neutrality less than 0.008e. Such a low value is a good indicator for an adequate convergence of the calculations.

The second quantum mechanical DFT package program used in the calculations is ABINIT code [24, 25]. The exchange-correlation energy function in this package program is treated within the local density approximation (LDA) [26] by the density functional of Ceperley and Alder [27]. To get a good convergence in the calculations, the kinetic energy cutoff is found to be 28 Hartree, using a $8 \times 8 \times 8$ Monkhorst–Pack [23] mesh grid for the Brillouin zone sampling of special k points.

Table 1. The calculated equilibrium lattice parameters (*a*, *b*, and *c*) together with the experimental values and electronic band gaps for $Sn_2P_2S_6$.

Material	Pressure	*a* (Å)	*b* (Å)	*c* (Å)	*β*	V_0 (Å^3)	E_g (eV)	Refs.
$Sn_2P_2S_6$-Pc	0 GPa	6.656	7.707	11.818	123.93	502.95	2.12 (I)	Present
		6.529	7.485	11.317	124.11	457.91	–	Exp. [5]
							2.20 (I)	WIEN2k [9]
							2.3 (D)	Exp. [29]
	20 GPa	5.898	6.776	10.356	123.5	344.63	0.7 (I)	Present
	40 GPa	5.552	6.549	9.777	122.9	298.64	Semi-metal	Present
$Sn_2P_2S_6$-P2_1/c	0 GPa	6.626	7.702	11.400	124.06	482.01	1.74 (I)	Present
		6.518	7.463	11.267	124.22	453.183		Exp. [28]
	20 GPa	5.898	6.784	10.346	123.5	344.65	0.7 (I)	Present

3. Results and Discussion

3.1. Structural Properties

We investigated structural properties of $Sn_2P_2S_6$ compound in Pc space group ferroelectic and P2_1/c space group paraelectric phases. The total energy is calculated to determine the physical properties of a material. The optimization process is performed to calculate this total energy. The lattice parameters have been calculated in the optimization process using the experimental lattice parameters and atomic positions given at Refs. [5, 28]. The lattice parameters calculated for both phases of the $Sn_2P_2S_6$ compound are given in Table 1. The calculated lattice parameters are in agreement with the experimental values. We wanted to get an idea of the changes in structural, mechanical and electronic properties by applying pressure to both phases of the $Sn_2P_2S_6$ compound. Structural values of both phases have been calculated at 20 GPa. The angles β have the same value while the lattice parameter values are very close to each other. The optimization process at 40 GPa has not been successful in the paraelectric phase but successful in the ferrolectic phase. It has been seen that the $Sn_2P_2S_6$ compound from the electronic band structure calculated in ferrolectic phase (Pc) at 40 GPa has passed from semiconductor structure to semi-metal structure (see Table 1). It is understood that the $Sn_2P_2S_6$ compound undergoes phase transition at a value close to 40 GPa. Therefore, it is an expected result that the lattice parameter values due to increased pressure applied are close to each other.

3.2. Elastic Properties

We calculated the elastic constants for both phases of the $Sn_2P_2S_6$ compound using the strain-stress method [30]. The obtained elastic constants for both phases are given in Table 2. The calculated elastic constants provide the mechanical stability criteria given in Refs. [31,32]. The elastic constants C_{11}, C_{22} and C_{33} in monoclinic crystals measure the a-, b- and c-direction resistance to linear compression, respectively. For both phases of the $Sn_2P_2S_6$ compound, the elastic constant C_{11} at 0 GPa is greater than C_{22} and C_{33}. At different pressures (20 GPa for paraelectric phase and 20, 40 GPa for paraelectric phase), the elastic constant C_{33} in both phases is greater than C_{11} and C_{22}. Therefore, the $Sn_2P_2S_6$ compound in both phases can be more highly compressible in the b and c directions at 0 GPa, and more highly compressible in the a and b directions at different

Table 2. The calculated elastic constants (in GPa) for $Sn_2P_2S_6$.

Material	Pressure	C_{11}	C_{12}	C_{13}	C_{15}	C_{22}	C_{23}	C_{25}	C_{33}	C_{35}	C_{44}	C_{46}	C_{55}	C_{66}
$Sn_2P_2S_6$-Pc	0	120.0	40.6	28.6	−19.3	86.6	32.7	0.3	123.2	5.7	49.3	1.4	40.9	38.3
	20	252.4	89.5	63.7	−30.5	186.7	95.2	−0.7	248.4	20.6	101.0	4.4	111.8	85.4
	40	341.2	125.2	87.4	−32.2	250.2	147.1	1.2	318.2	27.5	135.4	6.3	162.8	114.7
$Sn_2P_2S_6$-P2_1/c	0	129.1	43.8	30.4	−24.7	92.8	34.2	−0.2	126.6	9.9	53.6	0.1	42.5	50.0
	20	252.2	89.5	63.5	−30.6	187.1	95.3	−0.7	247.8	20.1	100.9	4.4	111.8	85.4

Table 3. The calculated isotropic bulk modulus (B, in GPa), shear modulus (G, in GPa), Young's modulus (E, in GPa) and Poisson's ratio for $Sn_2P_2S_6$.

Material	Pressure	B_R	B_V	B_H	G_R	G_V	G_H	E	υ	G/B	B/G
$Sn_2P_2S_6$-Pc	0	58.0	59.3	58.7	37.6	40.9	39.3	96.3	0.23	1.49	0.67
	20	130.6	131.6	131.1	81.1	88.9	85.0	209.7	0.23	1.54	0.65
	40	180.4	181.0	180.7	104.9	119.2	112.1	278.6	0.24	1.61	0.62
$Sn_2P_2S_6$-P2_1/c	0	61.5	62.8	62.2	40.2	45.2	42.7	104.3	0.22	1.46	0.69
	20	130.6	131.5	131.1	81.1	88.9	85.0	209.6	0.23	1.54	0.65

pressures. Unfortunately, the experimental and theoretical values to compare our results were not found.

Using calculated elastic constants, bulk (B) and shear (G) modules have been obtained from Voigt (V)–Reuss (R)–Hill (H) approaches [33–35]. The Young's modulus, Poisson's ratio, anisotropic factors, sound velocity and Debye temperature have been also calculated from the obtained bulk and shear modules. The calculated bulk modulus, shear modulus, Young modulus and Poisson ratio are given in Table 3. The bulk modulus is a measure of resistance to volume change under applied pressure. The shear modulus is the material's response to shear stress and is a measure of the resistance to reversible deformations. The bulk (B_H) and shear (G_H) moduli obtained for the ferroelectric and paraelectric phases are 58.7 GPa, 62.2 GPa and 39.3 GPa, 42.7 GPa respectively. As seen in Table 3, bulk and shear moduli showed a large increase due to pressure increase. Considering the value of Young's modulus ($E = 96.3$ GPa and $E = 104.3$ GPa for ferroelectric phase and paraelectric phase, respectively), which is a measure of stiffness, we can say that these materials are stiff. At zero pressure, the paraelectric phase is stiffer than the ferroelectric phase. In both phases, the value of E with the increase in pressure also increases and is the same value at 20 GPa (see Table 3). The value of the Poisson's ratio is always 0.1 for covalent materials and 0.25 for ionic materials [36–38]. The Poisson's ratio (υ) values calculated for ferroelectric phase and paraelectric phase at zero pressure are 0.23 and 0.22, respectively. Thus, the ionic character is dominant in the atomic bonds of both phases. The dominant ionic character in both phases does not change with increasing pressure. If the B/G ratio is less (high) than 1.75, the material is brittle (ductile) [39, 40]. $Sn_2P_2S_6$ compound at both phases are therefore brittle. As the pressure increases, a change from brittle to ductility is observed.

The calculated anisotropic factors, sound velocities [41–43] and Debye temperatures are given in Table 4. For a completely isotropic system, $A = 1$. Deviation from the unity measures the degree of anisotropic. The A_1, A_2 and A_3 values calculated for ferroelectric and paraelectric are 1.06, 1.13, 1.22 and 1.10, 1.13, 1.49, respectively. There has been a significant increase in the value of A_2 with increasing pressure. The percentage of anisotropy in the compression and shear are defined as $A_{\text{comp}} = (B_V - B_R)/$

Table 4. The calculated anisotropic factors, sound velocities (υ_t, υ_l, υ_m), the Debye temperatures for $Sn_2P_2S_6$.

Material	Pressure	A_1	A_2	A_3	A_{comp} (%)	A_{shear} (%)	v_t (m/s)	v_l (m/s)	v_m (m/s)	θ_D (K)
$Sn_2P_2S_6$-Pc	0	1.06	1.13	1.22	1.07	4.15	3479	5850	3852	392
	20	1.08	1.83	1.31	0.37	4.57	4235	7182	4693	541
	40	1.12	2.38	1.35	0.16	6.40	4527	7770	5022	607
$Sn_2P_2S_6$-P2_1/c	0	1.10	1.13	1.49	1.03	5.90	3550	5930	3928	405
	20	1.08	1.83	1.31	0.36	4.58	4234	7181	4692	541

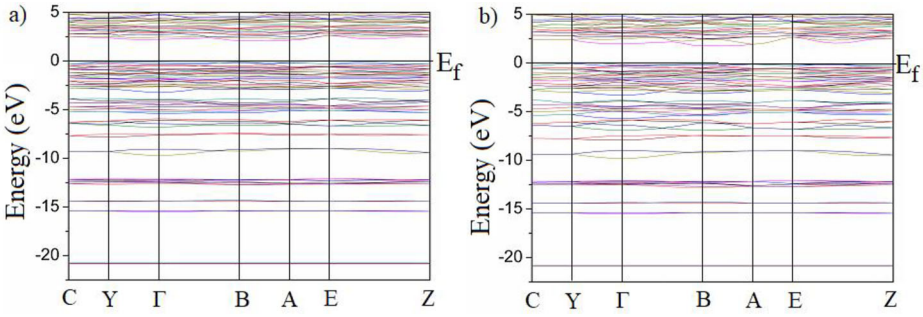

Figure 1. Energy band structure for (a) $Sn_2P_2S_6$-Pc and (b) $Sn_2P_2S_6$-P2_1/c.

$(B_V + B_R) \times 100$ and $A_{shear}=(G_V - G_R)/(G_V + G_R) \times 100$ [44,45]. While showing 0% value isotropy, 100% value indicates elastic anisotropy. The A_{comp} and A_{shear} values calculated for ferroelectric and paraelectric are 1.07, 4.05 and 1.03, 5.90, respectively. In the paraelectric phase, with the increase of pressure, A_{comp} decreases and A_{shear} increases. In the ferroelectric phase, both A_{comp} and A_{shear} decrease. In general, the Debye temperature is small for soft materials and large for hard materials. The Debye temperature value (405 K) of the paraelectric phase is greater than the ferroelectric phase (392 K). From the Debye temperature value, it is understood that the paraelectric phase of $Sn_2P_2S_6$ is stiffer than the ferroelectric phase. These results are consistent with results of the Young's module. The Debye temperature value with increasing pressure increases for both phases.

3.3. Electronic Properties

The electronic band structures for the ferroelectric (Pc) and paraelectric (P2_1/c) phases of the $Sn_2P_2S_6$ compound along the high symmetry points in space k have been calculated. The results are given in Figure 1. E_f is drawn to zero energy level in the figure graph. As can be seen from band structures at zero pressure, the forbidden energy band gap value (E_g) obtained for ferroelectric and paraelectric phases is 2.12 eV and 1.74 eV, respectively. As shown in Figure 1, the maximum of the valence band between Y-G in both phases is slightly closer to the Y high symmetry point, while the minimum of conductivity band between B-A is slightly closer to the point A in ferroelectric phase and point B in paraelectric phase. Therefore, E_g has indirect character in both phases. The calculated E_g values for the ferroelectric phase and paraelectric are in agreement with the experimental and theoretical values [9, 29, 46]. In both phases of the $Sn_2P_2S_6$ compound, the E_g values as with the results of [46] decrease due to the increase in pressure.

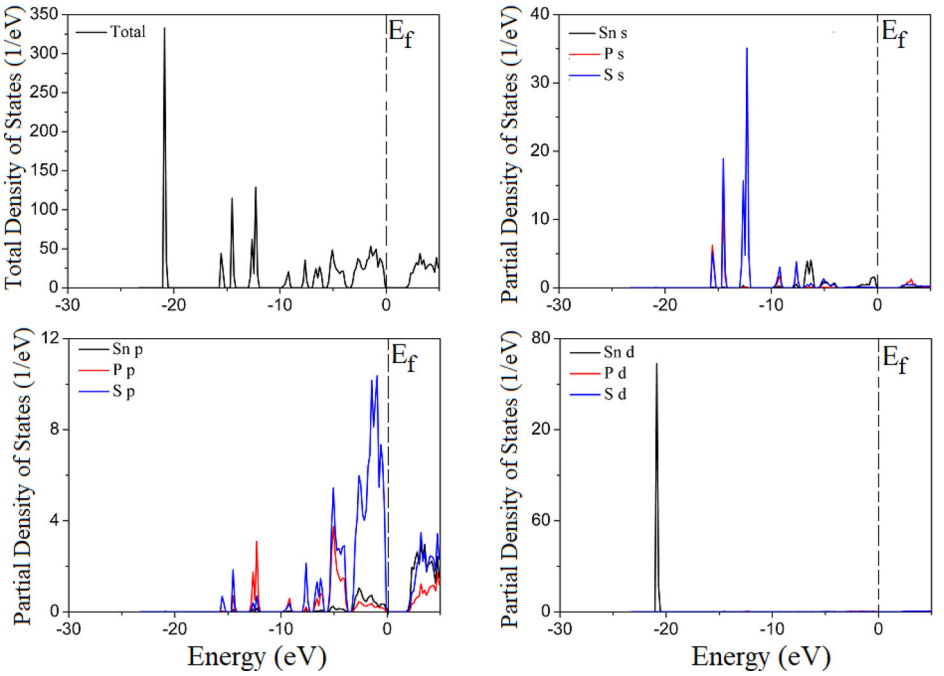

Figure 2. The total and projected density of states for $Sn_2P_2S_6$-Pc.

It is understood that the ferroelectric phase of the $Sn_2P_2S_6$ compound at 40 GPa undergoes a phase transition from the semiconductor structure to the semi-metal structure.

The total and partial density of states corresponding to the electronic band structure for both phases of the $Sn_2P_2S_6$ compounds at zero pressure have been calculated and are given in Figures 2 and 3. DOS figures of both phases of the $Sn_2P_2S_6$ compound exhibit similar behavior. The lowest valence bands, bands between −16 and 12 eV, bands between −10 and 3 eV and bands between −3 and 0 eV are occupied by the Sn d states, predominantly the S s states, predominantly the S p + P p states and predominantly the S p states, respectively. The conductivity bands just above the Fermi level are occupied by the states p of all three elements.

3.4. Optical Properties

3.4.1. Linear optical response

It is well known that the effect of the electric field vector, $E\ (\omega)$, of the incoming light is to polarize the material. In an insulator the polarization can be expressed as a Taylor expansion of the $E\ (\omega)$

$$P^i(\omega) = P_s^i + \sum_{j=1}^{3} \chi_{ij}^{(1)}(-\omega,\omega)E^j\left(\omega\right) + \sum_{j,l=1}^{3} \chi_{ijl}^{(2)} E^j(\omega)E^l(\omega) + \ldots, \tag{1}$$

where P^i is the zero field (spontaneous) polarization, $\chi_{ij}^{(1)}$ is the linear optical susuceptibility tensor and is given by Ref. [47].

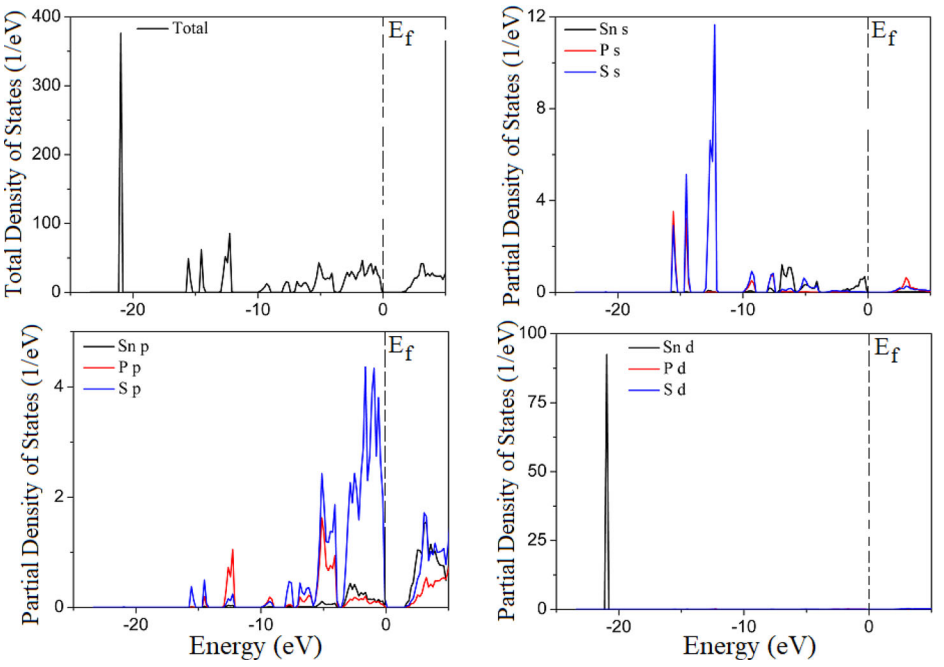

Figure 3. The total and projected density of states for $Sn_2P_2S_6$-P2_1/c.

$$\chi_{ij}^{(1)}(-\omega,\omega)=\frac{e^2}{\hbar\omega}\sum_{n,m,\vec{K}} f_{nm}(\vec{K})\frac{r_{nm}^{i}(\vec{K})r_{mn}^{j}(\vec{K})}{\omega_{mn}(\vec{K})-\omega}=\frac{\varepsilon_{ij}(\omega)-\delta_{ij}}{4\pi}, \tag{2}$$

where n, m denote energy bands, $f_{mn}(\vec{K})=f_m(\vec{K})-f_n(\vec{K})$ is the Fermi occupation factor, and Ω is normalization volume.

$\omega_{mn}(\vec{K})=\left[\omega_m(\vec{K})-\omega_n(\vec{K})\right]$ is the frequency difference and $\hbar\omega_n(\vec{K})$ is the energy of band n at wave vector $\vec{K}$. The *rijk* are the matrix elements of the position operator and given by

$$r_{nm}^{i}(\vec{K})=\frac{v_{nm}^{i}(\vec{K})}{i\omega_{nm}};\ \ \omega_n\neq\omega_m$$
$$r_{nm}^{i}(\vec{K})=0;\ \ \omega_n=\omega_m \tag{3}$$

where $v_{nm}^{i}(\vec{K})=\left[P_{nm}^{i}(\vec{K})/m\right]$. m is the free electron mass, and P_{nm} is the momentum matrix element. $\chi_{ijl}^{(2)}$ is the second-order nonlinear susceptibility tensor. As can be seen from Eq. (2), the dielectric function $\varepsilon_{ij}(\omega)=\left[1+4\pi\chi_{ij}^{(1)}(-\omega,\omega)\right]$ and the imaginary part of $\varepsilon_{ij}(\omega)$, $\varepsilon_2^{ij}(\omega)$ is given by

$$\varepsilon_2^{ij}(\omega)=\frac{e^2}{\hbar\pi}\sum_{nm}\int d\vec{K}f_{nm}(\vec{K})\frac{v_{nm}^{i}(\vec{K})v_{mn}^{j}(K)}{\omega_{mn}^{2}}\delta(\omega-\omega_{mn}(K)) \tag{4}$$

The real part of $\varepsilon_{ij}(\omega)$, $\varepsilon_1^{ij}(\omega)$ can be obtained by using Kramers–Kronig transformation

$$\varepsilon_1^{ij}(\omega) - 1 = \frac{2}{\pi} P \int_0^{\infty} \frac{\omega' \varepsilon_2^{ij}(\omega')}{\omega'^2 - \omega^2} d\omega' \tag{5}$$

As the Kohn–Sham equations only determine the ground-state properties, hence the unoccupied conduction bands have no physical significance. If they are used as single-particle states in the optical calculation of semiconductors, a band gap problem comes into existence: The absorption starts at an excessively low energy [48]. In order to remove the deficiency the many-body effects must be included in calculations of response functions. In order to take into account the self-energy effects, the scissors approximation is generally used [49]. In the calculation of the optical response in present work we have used the standard expression for $\varepsilon_{ij}(\omega)$ (see Eqs. 4 and 5).

3.4.2. Nonlinear response

The general expression of the nonlinear optical susceptibility depends on the frequencies of the $E(\omega)$. Therefore, in present context of the $(2n+1)$ theorem applied within the LDA to DFT we get an expression for the second order susceptibility [48–52]. As the sum of the three physically different contributions

$$\chi_{ijl}^{(2)}(-\omega_\beta, -\omega_\gamma, \omega_\beta, \omega_j) = \overset{''}{\chi}_{ijl}(-\omega_\beta, -\omega_\gamma; \omega_\beta, \omega_j) + \overset{''}{\eta}_{ijl}(-\omega_\beta, -\omega_j, \omega_\beta, \omega_j) + i\frac{\overset{''}{\sigma}_{ijl}(-\omega_\beta, -\omega_j, \omega_\beta, -\omega_\gamma)}{\omega_\beta + \omega_\gamma} \tag{6}$$

That includes contributions of interband and intraband transitions to the second order susceptibility. The first term in Eq. (6) describes contribution of inter band transitions to second order susceptibility. The second term represents the contribution of intraband transitions to second order susceptibility and the third term is the modulation of interband terms by intrabands terms. We used this expression to calculate the nonlinear response functions of $Sn_2P_2S_6$ ferroelectrics.

The fact that the nonlinear second harmonic generation (SHG) coefficients are related to the optical transitions has remarkable consequences. First of all, we note that equations for SHG consist of a number of resonant terms. In this sense, the imaginary part, $\mathrm{Im}\chi^{(2)}(-2\omega, \omega, \omega)$ resembles the $\varepsilon_2(\omega)$ and provides a link to the band structure. The difference, however, is that whereas in $\varepsilon_2(\omega)$ only the absolute value of the matrix elements squared enters, the matrix m elements entering the various terms in $\chi^{(2)}$ are more varied. They are in general complex and can have any sign. Thus $\mathrm{Im}\chi^{(2)}(-2\omega, \omega, \omega)$ can be both positive and negative. Second, there appear both resonances when 2ω equals an interband energy. Figure 4 shows the 2ω and single ω resonances contributions to $\mathrm{Im}\chi^{(2)}(-2\omega,\omega,\omega)$ compared to $\varepsilon_2(\omega)$. They clearly show a greater variation from high symmetry to lowest symmetry than the linear optical response. In some sense, they resemble a modulated spectrum. Third, we note that the 2ω resonances occur at half the frequency corresponding to the interband transition.

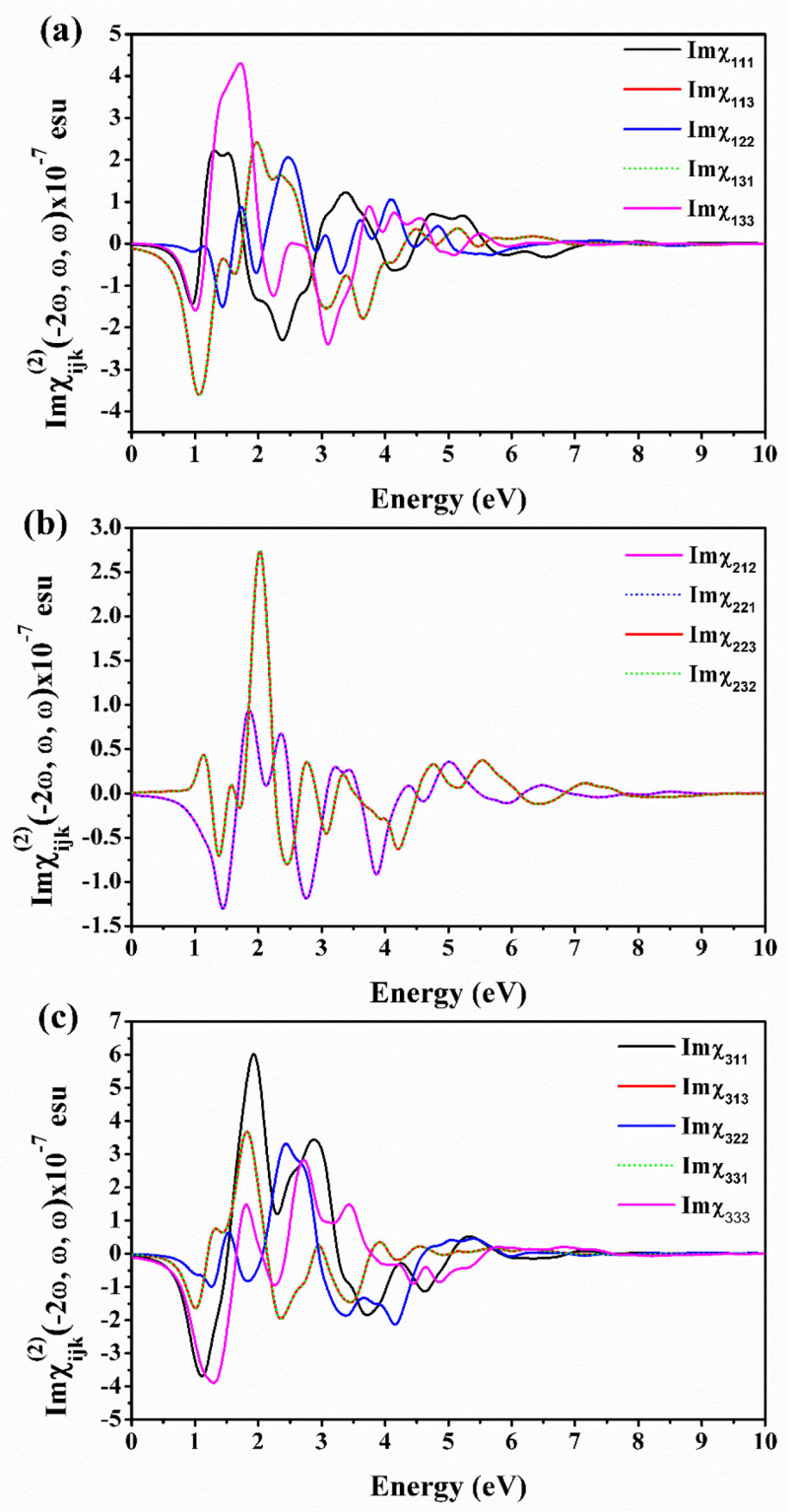

Figure 4. Total second-order susceptibility $Im\chi^{(2)}_{ijk}(-2\omega,\ \omega,\omega)$ for $Sn_2P_2S_6$-Pc compound.

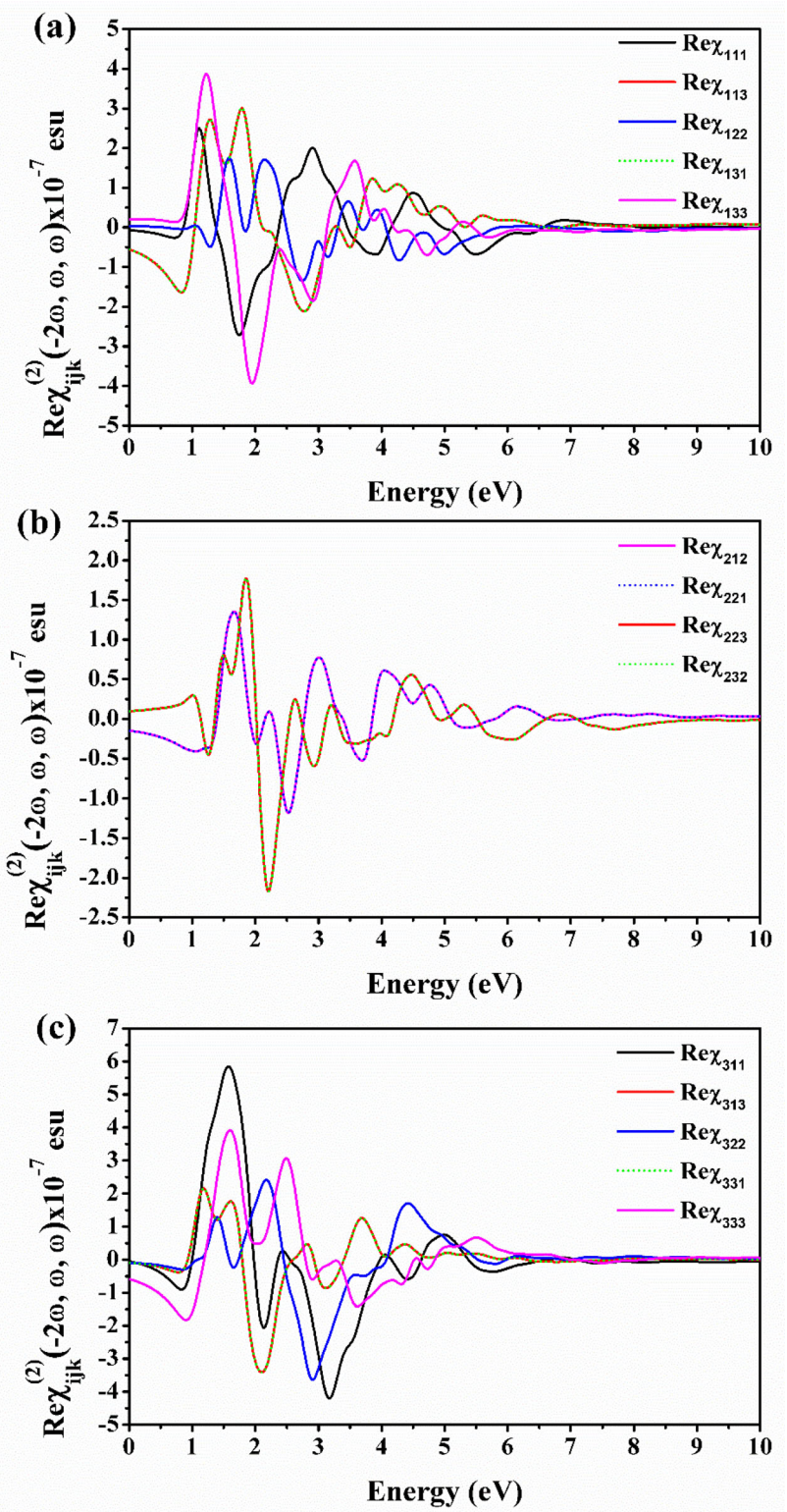

Figure 5. Total second-order susceptibility $Re\chi^{(2)}_{ijk}(-2\omega,\ \omega, \omega)$ for $Sn_2P_2S_6$-Pc compound.

Table 5. The Calculated intraband and interband of the zero frequency of $Re\chi^{(2)}_{ijk}(0)$ for $Sn_2P_2S_6$-Pc compound.

$Re\chi^{(2)}_{ijk}(0)$	Inter(1ω)	Inter(2ω)	Intra(1ω)	Intra(2ω)
$\chi_{111}(\omega)$	−0.3132	1.1929	0.3240	−1.2789
$\chi_{113}(\omega) = \chi_{131}(\omega)$	−1.5218	2.2299	0.8674	−2.1307
$\chi_{122}(\omega)$	−0.2382	−0.2239	0.1121	0.3852
$\chi_{133}(\omega)$	−0.4177	0.6063	0.4588	−0.4487
$\chi_{212}(\omega) = \chi_{221}(\omega)$	0.1319	−0.5964	−0.2457	0.5627
$\chi_{223}(\omega) = \chi_{232}(\omega)$	0.7498	−1.4575	−0.9018	1.7065
$\chi_{311}(\omega)$	0.2436	0.4862	−0.5944	−0.1930
$\chi_{313}(\omega) = \chi_{331}(\omega)$	−0.0949	0.3026	−0.1295	−0.1680
$\chi_{322}(\omega)$	−1.5216	0.7978	1.0429	−0.4127
$\chi_{333}(\omega)$	−1.2579	3.1496	0.8349	−3.3112

This is important for semiconductor/ferroelectric materials like $Sn_2P_2S_6$ compound where laser light sources reaching the higher interband transitions are not available. Nevertheless, one still needs to be able to detect the corresponding 2ω signal in the UV. Unfortunately, the intrinsic richness of $\chi^{(2)}$ spectra remains largely to be explored experimentally we are not aware of any attempts to measure both the real and imaginary parts of the these spectral functions as one standard does in linear optics. That is attributed to the fact that the second harmonic response $\chi_{ijk}{}^{(2)}(\omega)$ contains 2ω resonance along with the usual ω resonance. Both the ω and resonances can be further separated into inter-band and intra-band contributions. The structure in $\chi_{ijk}{}^{(2)}(\omega)$ can be understood from the structures in $\varepsilon_2(\omega)$. Our calculations for $\varepsilon_2(\omega)$ give few fundamental oscillators between 1.0 eV and 6.0 eV which correspond to the optical transitions from the valance bands to the conduction band, formed by the d orbits of the Ta atoms and consisting of two subbands. It is well known that the $\varepsilon_2(\omega)$ function computed from moments (**p**) appear to be very sensitive to the ab initio parameters and seem to be particularly appropriate to test electronic band structure. In $Sn_2P_2S_6$ compound the two peak present in experimental reflectivity data are obtained in theoretical curves only when the interband transition moments varied with respect to the energies and k wave vectors. The structure 0.5–3.0 eV in $\chi_{\mathrm{ijk}}{}^{(2)}(\omega)$ is associated with interference between ω and 2ω resonances, while the structure above 2.0 eV is due to mainly to ω resonance. In Figure 5, we show the 2ω interband and intraband contributions for $Sn_2P_2S_6$ compound. Also given is their decomposition into intra- and interband contributions.

Note that the interband part are negative in all cases and in most cases largely compensate the intraband part. Our compounds in both cases of which interband part is much smaller in magnitude than the intraband part. This quite interesting because unexpected. We investigated the reasons for the cancelation of intra- and interband parts by inspecting the corresponding frequency dependent imaginary parts of the $\chi^{(2)}$ $(-2\omega, \omega, \omega)$. First of all, one now sees that the opposite sign of intra- and interband parts not only occurs in the static value but occurs almost energy by energy. The sign of the inter and intraband part are difficult to understand *a priori* because a variety of matrix element products comes into play and both ω and 2ω resonances occur in both the pure interband, and the interband contribution modified by intra-band motion when these are further worked out into separate resonance terms. As an example of

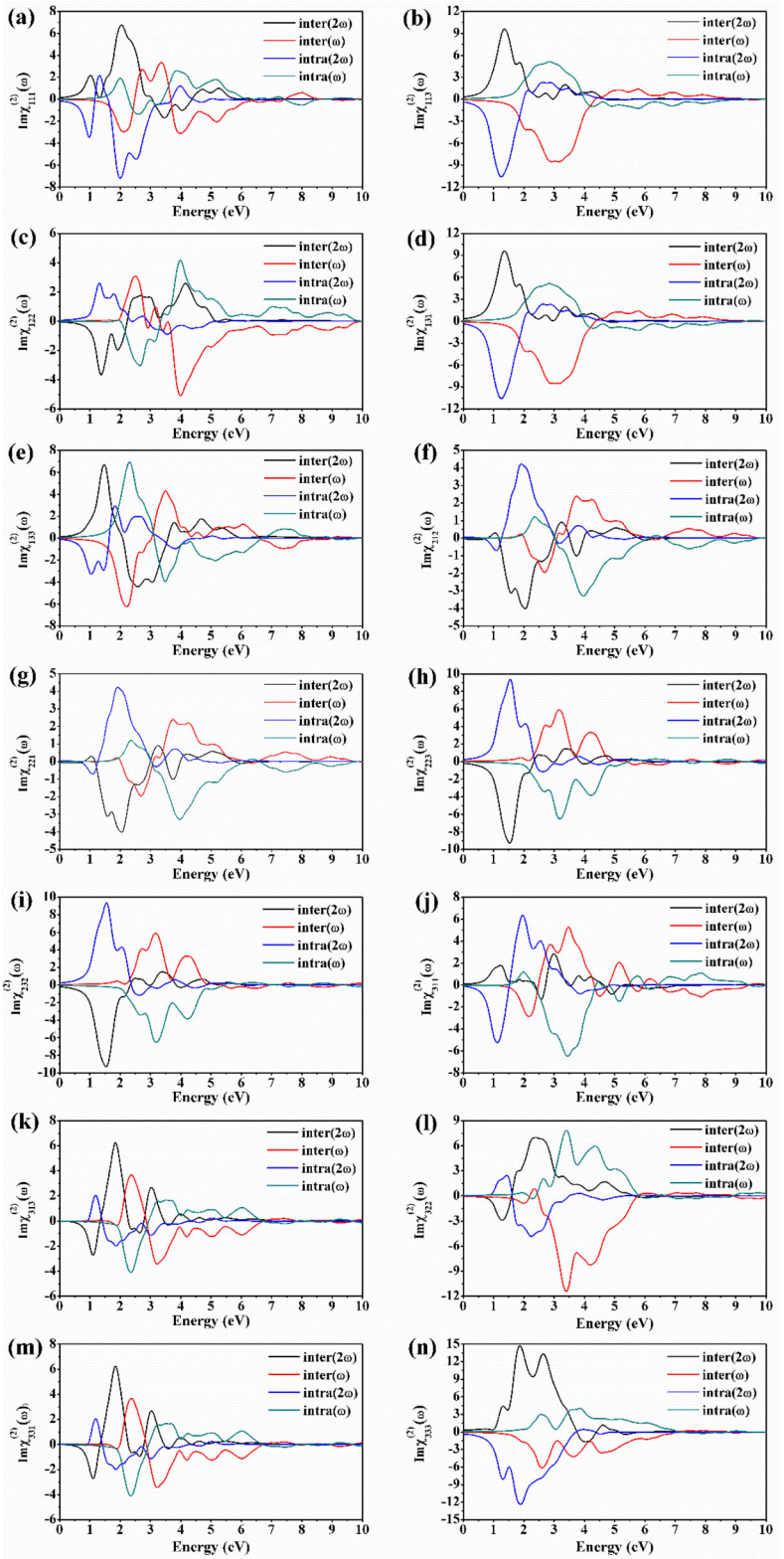

Figure 6. The calculated $Im\chi^{(2)}_{ijk}(\omega)$ with the intraband and interband contributions for $Sn_2P_2S_6$-Pc compound.

such a prediction the SHG coefficients of $Sn_2P_2S_6$ compound are given in Table 5 (see Figure 6). For incident light with a frequency small compared to the energy gap. The independent tensor components are listed for $\omega = 0$.

4. Conclusion

The structural, elastic, electronic, linear and nonlinear optical properties under high pressure for the $Sn_2P_2S_6$ compound using the density functional methods in generalized gradient approximation have been calculated over a wide energy range. This allowed us to study the trends in the second order optical response with chemical composition. The results for the zero-frequency limit of second harmonic generation in agreement with available experimental and theoretical results for $Sn_2P_2S_6$. For all the considered compounds the SHG coefficient $\chi^{(2)}$ is of the order of $\sim 10^{-7}$ esu. Our calculations of the SHG susceptibility show that the intra-band and interband contributions are significantly changes with pressure.

Funding

This work is supported by the projects DPT-HAMIT and NATO-SET-193. One of the authors (Ekmel Ozbay) acknowledges partial support from the Turkish Academy of Sciences.

References

1. H. Hahn and W. Klingen, Über einige ternäre Verbindungen vom Typ des Arsenopyrits, *Naturwissenschaften* **52** (17), 494 (1965). DOI: 10.1007/BF00646575.
2. R. Nitsche and P. Wild, Crystal growth of metal–phosphorus–sulfur compounds by vapor transport, *Mater. Res. Bull.* **5** (6), 419 (1970). DOI: 10.1016/0025-5408(70)90080-2.
3. W. Klingen, R. Ott, and H. Hahn, Uber die Darstellung und Eigenschaften von Hexathio- und Hexaselenohypodiphosphaten, *Z. Anorg. Allg. Chem.* **396** (3), 271 (1973). DOI: 10.1002/zaac.19733960305.
4. G. Dittmar and H. Schafer, Die Struktur des Di-Zinn-Hexathiohypodiphosphats $Sn_2P_2S_6$, *Z. Naturforsch. B* **29** (5–6), 312 (1974). DOI: 10.1515/znb-1974-5-603.
5. C. D. Carpentier and R. Nitsche, Ferroelectricity in $Sn_2P_2S_6$, *Mater. Res. Bull.* **9** (8), 1097 (1974). DOI: 10.1016/0025-5408(74)90023-3.
6. B. Scott *et al.*, High temperature crystal structure and DSC of $Sn_2P_2S_6$, *J. Solid State Chem.* **96** (2), 294 (1992). DOI: 10.1016/S0022-4596(05)80262-2.
7. I. Zamaraite *et al.*, Double hysteresis loops in proper uniaxial ferroelectrics, *Phys. Rev. Appl.* **10** (3), 034017 (2018). DOI: 10.1103/PhysRevApplied.10.034017.
8. K. Kuepper *et al.*, Electronic structure of $Sn_2P_2S_6$, *Phys. Rev. B.* **67** (11), 11501 (2003). DOI: 10.1103/PhysRevB.67.115101.
9. Y. Li and D. J. Singh, Properties of the ferroelectric visible light absorbing semiconductors: $Sn_2P_2S_6$ and $Sn_2P_2Se_6$, *Phys. Rev. Mater.* **1** (7), 075402 (2017). DOI: 10.1103/PhysRevMaterials.1.075402.
10. J. Grigas *et al.*, XPS of electronic structure of ferroelectric $Sn_2P_2S_6$ crystals, *Ferroelectrics* **378** (1), 70 (2009). DOI: 10.1080/00150190902845145.
11. K. Glukhov *et al.*, Electronic structure and phase transition in ferroelectric $Sn_2P_2S_6$ crystal, *Int. J. Mol. Sci.* **13** (11), 14356 (2012). DOI: 10.3390/ijms131114356.
12. Y. Rong *et al.*, Large negative thermal expansion in non-perovskite lead-free ferroelectric $Sn_2P_2S_6$, *Phys. Chem. Chem. Phys.* **18** (8), 6247 (2016). DOI: 10.1039/C6CP00011H.

13. M. B. Smirnov, J. Hlinka, and A. V. Solov'ev, Lattice dynamics and the ferroelectric phase transition in $Sn_2P_2S_6$, *Phys. Rev. B* **61** (22), 15051 (2000). DOI: 10.1103/PhysRevB.61.15051.
14. I. P. Studenyak *et al.*, Temperature variation of optical absorption edge in $Sn_2P_2S_6$ and SnP_2S_6 crystals, *Ferroelectrics* **254** (1), 295 (2001). DOI: 10.1080/00150190108215009.
15. Y. M. Vysochanskii *et al.*, Mössbauer 119Sn and XPS spectroscopy of $Sn_2P_2S_6$ and SnP_2S_6 crystals, *Phys. Stat. Sol. (b)* **246** (5), 1110 (2009). DOI: 10.1002/pssb.200844316.
16. Y. Vysochanskii *et al.*, Ferroelectric and semiconducting properties of $Sn_2P_2S_6$ crystals with intrinsic vacancies, *Ferroelectrics* **418** (1), 124 (2011). DOI: 10.1080/00150193.2011.578979.
17. P. Hohenberg and W. Kohn, Inhomogeneous electron gas, *Phys. Rev.* **136** (3B), B864 (1964). DOI: 10.1103/PhysRev.136.B864.
18. G. Kresse and J. Hafner, Ab initio molecular dynamics for liquid metals, *Phys. Rev. B Condens. Matter* **47** (1), 558 (1993). DOI: 10.1103/physrevb.47.558.
19. G. Kresse and J. Furthmüller, Efficiency of ab-initio total energy calculations for metals and semiconductors using a plane-wave basis set, *Comput. Mater. Sci.* **6** (1), 15 (1996). DOI: 10.1016/0927-0256(96)00008-0.
20. G. Kresse and D. Joubert, From ultrasoft pseudopotentials to the projector augmented-wave method, *Phys. Rev. B* **59** (3), 1758 (1999). DOI: 10.1103/PhysRevB.59.1758.
21. G. Kresse and J. Furthmüller, Efficient iterative schemes for ab initio total-energy calculations using a plane-wave basis set, *Phys. Rev. B Condens. Matter* **54** (16), 11169 (1996). DOI: 10.1103/PhysRevB.54.11169.
22. J. P. Perdew, K. Burke, and M. Ernzerhof, Generalized gradient approximation made simple, *Phys. Rev. Lett.* **77** (18), 3865 (1996). DOI: 10.1103/PhysRevLett.77.3865.
23. H. J. Monkhorst and J. D. Pack, Special points for Brillouin-zone integrations, *Phys. Rev. B* **13** (12), 5188 (1976). DOI: 10.1103/PhysRevB.13.5188.
24. X. Gonze *et al.*, First-principles computation of material properties: the ABINIT software project, *Comput. Mater. Sci.* **25** (3), 478 (2002). DOI: 10.1016/S0927-0256(02)00325-7.
25. X. Gonze *et al.*, ABINIT: first-principles approach to material and nanosystem properties, *Comput. Phys. Commun.* **180** (12), 2582 (2009). DOI: 10.1016/j.cpc.2009.07.007.
26. R. Cohen and H. Krakauer, Lattice dynamics and origin of ferroelectricity in $BaTiO_3$: linearized-augmented-plane-wave total-energy calculations, *Phys. Rev. B Condens. Matter* **42** (10), 6416 (1990). DOI: 10.1103/physrevb.42.6416.
27. D. M. Ceperley and M. J. Adler, Ground state of the electron gas by a stochastic method, *Phys. Rev. Lett.* **45** (7), 566 (1980). DOI: 10.1103/PhysRevLett.45.566.
28. Y. V. Voroshilov *et al.*, Crystal structure of $Sn_2P_2S_6$, *Ukr. Fiz. Zh. (Russ. Ed.)* **35**, 71 (1990).
29. A. Ruediger *et al.*, Studies of light-induced charge transfer in $Sn_2P_2S_6$ by combined EPR/optical absorption spectroscopy, *Opt. Mater.* **18** (1), 123 (2001). DOI: 10.1016/S0925-3467(01)00147-1.
30. Y. L. Page and P. Saxe, Symmetry-general least-squares extraction of elastic coefficients from ab initio total energy, *Phys. Rev. B* **63** (17), 174103 (2001). DOI: 10.1103/PhysRevB.63.174103.
31. Z. J. Wu *et al.*, Crystal structure and elastic properties of superhard IrN_2 and IrN_3 from first principles, *Phys. Rev. B* **76** (5), 054115 (2007). DOI: 10.1103/PhysRevB.76.054115.
32. J. P. Watt and L. Peselnick, Clarification of the Hashin-Shtrikman bounds on the effective elastic moduli of polycrystals with hexagonal, trigonal, and tetragonal symmetries, *J. Appl. Phys.* **51** (3), 1525 (1980). DOI: 10.1063/1.327804.
33. W. Voight, *Lehrbook Der Kristallphysik* (Teubner, Leipsig, 1928), 962 pp.
34. A. Reuss, Berechnung der fließgrenze von mischkristallen auf grund der plastizitatsbedingung für einkristalle, *Z. Angew. Math. Mech.* **9** (1), 49 (1929). DOI: 10.1002/zamm.19290090104.
35. R. Hill, The elastic behavior of crystalline aggregate, *Proc. Phys. Soc. A* **65** (5), 349 (1952). DOI: 10.1088/0370-1298/65/5/307.
36. V. V. Bannikov, I. R. Shein, and A. L. Ivanovskii, Electronic structure, chemical bonding and elastic properties of the first thorium-containing nitride perovskite $TaThN_3$, *Phys. Stat. Sol. (RRL)* **1** (3), 89 (2007). DOI: 10.1002/pssr.200600116.

37. H. Koc *et al.*, Ab initio calculation of the structural, elastik, electronic, and linear optical properties of ZrPtSi and TiPtSi ternary compounds, *Comput. Mater. Sci.* **62**, 235 (2012). DOI: 10.1016/j.commatsci.2012.05.052.
38. H. Koc *et al.*, First principles prediction of the elastic, electronic, and optical properties of Sb_2S_3 and Sb_2Se_3 compounds, *Solid State Sci.* **14** (8), 1211 (2012). DOI: 10.1016/j.solidstatesciences.2012.06.003.
39. I. R. Shein and A. L. Ivanovskii, Elastic properties of mono- and polycrystalline hexagonal AlB_2-like diborides of s, p and d metals from first-principles calculations, *J. Phys. Condens. Matter* **20** (41), 415218 (2008). DOI: 10.1088/0953-8984/20/41/415218.
40. F. Pogh, Relations between the elastic moduli and the plastic properties of polycrystalline pure metals, *Philos. Mag.* **45**, 823 (1954). DOI: 10.1080/14786440808520496.
41. I. Johnston *et al.*, *Solids State Physics Simulations, the Consortium for Upper Level Physics Software* (Wiley, New York, 1996).
42. O. L. Anderson, A simplified method for calculating the Debye temperature from elastic constants, *J. Phys. Chem. Solids* **24** (7), 909 (1963). DOI: 10.1016/0022-3697(63)90067-2.
43. E. Schreiber, O. L. Anderson, and N. Soga, *Elastic Constants and Their Measurements* (McGraw-Hill, New York, 1973).
44. H. Zhai, X. Li, and J. Du, First-principles calculations on elasticity and anisotropy of tetragonal tungsten dinitride under pressure, *Mater. Trans.* **53** (7), 1247 (2012). DOI: 10.2320/matertrans.M2011373.
45. D. H. Chung and W. R. Buessem, *Anisotropy in Single Crystal Refractory Compounds* (Plenum, New York, 1968), 217 pp.
46. S. V. Ovsyannikov *et al.*, Tuning the electronic and vibrational properties of $Sn_2P_2Se_6$ and $Pb_2P_2S_6$ crystals and their metallization under high pressure, *Dalton Trans.* **46** (13), 4245 (2017). DOI: 10.1039/c6dt03854a.
47. E. Ghahramanı and J. E. Sipe, Full-band-structure calculation of epsilon, *Phys. Rev. B Condens. Matter* **46** (3), 1831 (1992). DOI: 10.1103/PhysRevB.46.1831.
48. S. C. Abrahamas *et al.*, Ferroelectric lithium tantalate—III. Temperature dependence of the structure in the ferroelectric phase and the para-electric structure at 940°K, *J. Phys. Chem. Solids* **34**, 521 (1973). DOI: 10.1016/0022-3697(73)90047-4.
49. W. G. Aulbur, L. Jonsson, and J. W. Wilkins, Quasiparticle calculations in solids, *J. Solid State Phys.* **54**, 1 (2000). DOI: 10.1103/PhysRevB.87.235132.
50. W. R. V. Lambrecht and S. N. Rashkeev, From band structures to linear and nonlinear optical spectra in semiconductors, *Phys. Stat. Sol. (b)* **217** (1), 599 (2000). DOI: 10.1002/3527603107.ch30.
51. A. H. Reshak, First-principle calculations of the linear and nonlinear optical response for GaX (X = As, Sb, P), *Eur. Phys. J. B* **47** (4), 503 (2005). DOI: 10.1140/epjb/e2005-00364-3.
52. V. L. Gavrilenko, Ab initio theory of second harmonic generation from semiconductor surfaces and interfaces, *Phys. Stat. Sol. (a)* **188** (4), 1267 (2001). DOI: 10.1002/1521-396X(200112)188:4 < 1267::AID-PSSA1267 > 3.0.CO;2-2.